Extended application of a unified creep-ageing constitutive model to multistep heat treatment of aluminium alloys

Yong Li, Zhusheng Shi*, Jianguo Lin, Yo-Lun Yang and Qi Rong

Department of Mechanical Engineering, Imperial College London, London SW7 2AZ, UK

*Corresponding Author: Dr Zhusheng Shi (zhusheng.shi@imperial.ac.uk)

Abstract:

A recently developed unified constitutive model for creep-ageing of an Al-Cu-Li alloy (AA2050-T34) has been successfully extended to applications of multistep heat treatments of aluminium alloys, including natural and artificial ageing with simple and complex hardening evolution and creep-ageing with different initial temper conditions. An age hardening model for both natural and artificial ageing was proposed based on the unified creep-ageing constitutive model and methods to determine the initial and equilibrium values of both micro and macro variables of aluminium alloys under general heat-treated conditions were presented. By unifying normalised microstructural variables throughout the multistep heat treatments, the model was able to predict both the simple and complex strengthening evolution of various aluminium alloys during ageing and creep-ageing. A number of case studies were carried out for natural ageing, artificial ageing and creep-ageing of some typical heat-treatable aluminium alloys, including 2xxx (Al-Cu-Mg and Al-Cu-Li) and 7xxx (Al-Zn-Mg) alloys with as-quenched, naturally-aged (T3/T4) and peak-aged (T6/T8) initial temper conditions. Excellent agreement has been achieved between experimental and simulation results.

Keywords: Modelling; Ageing; Creep age forming; Aluminium alloy; Multistep heat treatment; Complex hardening behaviour

Nomenclature

Variables used in this paper

Variables	*Unit*	*Specification*
c, c_a, c_s	wt%	Solute concentration in the matrix, its equilibrium values at the ageing temperature and SHT temperature respectively
$\bar{c}$, $\bar{c}_a$	-	Normalised solute concentration and its equilibrium value at the ageing temperature
H	-	Creep variable
r, r_d, r_{n1}, r_{n2}	nm	Precipitate radius, its value for dissolving precipitates and new precipitates during natural ageing and artificial ageing respectively
r_{n1_x}, r_{n2_x}	nm	Radius of new precipitates of *x* (GP zones, θ', δ' etc.) from natural ageing and artificial ageing
t	h	Creep/ageing time
T	K	Temperature
β	-	Yield strength contribution coefficient from different precipitates (r_d, r_{n1} and r_{n2})
ε_{cr}	-	Creep strain
ρ, ρ_s	m^{-2}	Dislocation density and its saturated value
σ, σ_{ea}	MPa	Applied and effective applied stress respectively
σ_{dis}, σ_p, σ_{ss}	MPa	Contribution to yield strength from dislocations, precipitates and solid solution respectively
σ_d, σ_{n1}, σ_{n2}	MPa	Contribution to yield strength from dissolving precipitates and new precipitates during natural ageing and artificial ageing respectively
σ_{n1_x}, σ_{n2_x}	MPa	Contribution to yield strength from new precipitates of *x* (GP zones, θ', δ' etc.) during natural ageing and artificial ageing.
σ_{th_0}	MPa	Initial creep threshold stress
σ_y	MPa	Yield strength
X, $\bar{X}$, $\dot{X}$		Variable *X*, normalised *X*, time derivative of *X*
Subscripts X_c, X_0		Critical value and initial value of variable *X*

1. Introduction

Creep age forming (CAF) is a novel and promising forming technology to manufacture extra-large light weight and high performance panel products in the aerospace industry, in which strengthening of aluminium alloys from artificial ageing and plastic deformation from creep occur simultaneously at a proper ageing temperature [1]. The aluminium alloys used for the CAF process are heat-treated differently according to their particular compositions and corresponding specific industrial requirements, which will lead to different creep-ageing behaviour during their subsequent CAF process. Dunnwald and El-Magd [2] investigated creep behaviour of an Al-Cu-Mg alloys (AA2024) with as-quenched and over-aged initial tempers, and showed that the as-quenched material exhibited much stronger creep resistance compared with the over-aged one. The effects of initial tempers (including naturally-aged (T4) and peak-aged (T8)) of another Al-Cu-Mg alloy (AA2219) on springback after the CAF process were investigated by Lam et al. [3]. The results indicated that the peak-aged material would lead to more sprinbgack after the CAF process than the T4 material despite larger stress relaxation was observed in the former one. Different heat treatment histories also contributed to varying mechanical properties after creep-ageing of Al-Cu-Mg and Al-Zn-Mg-Cu alloys, as reported by Lin et al. [4, 5]. Li et al. [6] compared the creep-ageing behaviour of an Al-Cu-Li alloy (AA2050) with as-quenched, naturally-aged (T34) and peak-aged (T84) initial tempers. Both creep strain and yield strength variations behaved differently during creep-ageing in these three initial temper conditions.

Much effort has been made to model the heat treatment processes and different models have been proposed previously. Shercliff and Ashby [7] proposed a process model for artificial ageing of aluminium alloys and successfully predicted age hardening of some typical aluminium alloys with as-quenched and pre-aged initial temper conditions. Esmaeili et al. [8] developed a mechanism-based model for artificial ageing of AA6111, taking into account the evolution of both dissolving and nucleating precipitates. A practical model was proposed by Sha [9] to characterise the age hardening of several aluminium alloys (Al-Si-Cu and Al-Zn-Mg) at the early stage of artificial ageing. Artificial ageing of an over-aged Al-Zn-Mg-Cu alloy was also investigated and modelled by Starink and Wang [10]. On the basis of the developed models for artificial ageing, Raeisinia et al. [11] proposed a set of constitutive equations to predict the yield strength of AA6111 after multistep heat treatments, including both natural and artificial ageing. All these age hardening models concentrated on the alloys with comparatively simple yield strength evolution curves with the single-peak behaviour. However, some aluminium alloys with particular initial tempers, such as some Al-Cu-Mg [12], Al-Zn-Mg [13]

and Al-Cu-Li alloys [14], demonstrated more complex evolution of the yield strength, e.g., with a shoulder and a peak, but little has been done in modelling this type of behaviour.

For the CAF process, constitutive models were proposed to predict concurrent creep strain and age hardening for specified aluminium alloys with a particular initial temper. Ho et al. [15] proposed a model to predict creep-ageing of an as-quenched 7000 aluminium alloy. Part of the model was further applied to predict creep of some peak-aged alloys (AA7075-T651 and AA2124-T851) by Li et al. [16]. Different modelling methods and constitutive equations were used for creep-ageing of AA2024-T3 and AA7B04-T7451 alloys respectively by Lin et al. [17] and Li et al. [18]. Zhan et al. [19] developed a constitutive model for the CAF process of an as-quenched AA7055, considering strength contributions from dislocations, precipitates and solid solutes. The model was successfully applied to creep-ageing of some other aluminium alloys , such as AA2219 with T4 and T8 initial tempers [3] and AA7050 with T751 initial temper [20]. Recently a comprehensive unified constitutive model, based on some basic material models for creep and ageing, was developed to predict asymmetric tension and compression creep-ageing behaviour with the new double primary creep feature during creep-ageing of AA2050-T34 [21]. This model considered the evolution of normalised microstructural parameters (precipitate size, solute concentration, dislocation density) and their effects on hardening and creep deformation, and the predicted evolution of creep strain and yield strength agrees well with the experiments.

The aim of the study is to extend the application of the unified constitutive model to multistep heat treatments of various aluminium alloys, especially those with complex age hardening behaviour, as well as creep-ageing with different initial tempers. Methods to determine the initial and equilibrium values of material variables and a concept of unifying normalised microstructural variables throughout the multistep heat treatments are proposed. A number of case studies of the model application to both natural and artificial ageing and creep-ageing of various aluminium alloys with different initial tempers have been carried out and discussed.

2. Constitutive model

Current model is based on the unified constitutive model which successfully predicted the concurrent age hardening and creep of AA2050 during creep-ageing [21]. The whole set of constitutive model includes [21]:

$$\dot{\varepsilon}_{cr} = A_4 \sinh\left\{B_1\left((|\sigma| - \sigma_{th_0})(1-H)\right)\right\} sign(\sigma) \quad (1)$$

$$H = k_0\bar{\rho} + k_1\bar{c} + k_2(\bar{r}_n + \beta^{1/2}\bar{r}_d) \quad (2)$$

$$\dot{\bar{r}}_n = C_r(Q - \bar{r}_n)^{m_3}(1 + \gamma_0\bar{\rho}^{m_4}) \quad (3)$$

$$\dot{\bar{r}}_d = -\frac{C_{r1}}{\bar{r}_d} \quad (4)$$

$$\dot{\bar{c}} = -A_2(\bar{c} - \bar{c}_a)(1 + \gamma_0\bar{\rho}^{m_4}) \quad (5)$$

$$\dot{\bar{\rho}} = A_1(1-\bar{\rho})|\dot{\varepsilon}_{cr}|^{m_1} - C_p\bar{\rho}^{m_2} \quad (6)$$

$$\dot{\sigma}_{p-n} = C_a\dot{\bar{r}}_n^{m_5}(1 - \bar{r}_n^{m_6}) \quad (7)$$

$$\dot{\sigma}_{p-d} = C_{a1}\bar{r}_d^{m_7}\dot{\bar{r}}_d \quad (8)$$

$$\dot{\sigma}_{ss} = -C_{ss}\dot{\bar{c}}^{m_8}(\bar{c} - \bar{c}_a) \quad (9)$$

$$\dot{\sigma}_{dis} = A_3 n\bar{\rho}^{n-1}\dot{\bar{\rho}} \quad (10)$$

$$\sigma_y = \sigma_{ss} + \sqrt{\sigma_{dis}^2 + (\sigma_{p-d}^2 + \sigma_{p-n}^2)} \quad (11)$$

where $\dot{\varepsilon}_{cr}$ is the creep strain rate and H is a microstructure-controlled creep variable. $\bar{r}_n$, $\bar{r}_d$, $\bar{c}$ and $\bar{\rho}$ are the normalised microstructural variables representing the new precipitate radius, dissolving precipitate radius, solute concentration and dislocation density. The normalised dislocation density is defined as: $\bar{\rho} = (\rho - \rho_i)/\rho_s$ [21], where ρ_i is the initial dislocation density and ρ_s is the saturated dislocation density of the alloy during creep-ageing. σ_{p-n}, σ_{p-d}, σ_{ss} and σ_{dis} are the strength contributions to the yield strength (σ_y) of the alloy from new precipitates, dissolving precipitates, solutes and dislocations respectively.

As-quenched, naturally-aged (T3 or T4) and peak-aged (T6 or T8) tempers were all reported as suitable initial conditions for CAF of aluminium alloys [3, 6, 19]. An age hardening model to predict the evolution of the yield strength and microstructural variables of the alloys during these heat treatments, including natural and artificial ageing, can be simplified from the creep-ageing constitutive model by ignoring the creep related variables.

The yield strength (σ_y) of aluminium alloys during pure ageing is mainly determined by the contributions from the solid solution (σ_{ss}) (including the intrinsic strength of aluminium) and precipitation hardening (σ_p) [7], as:

$$\sigma_y = \sigma_{ss} + \sigma_p \quad (12)$$

The growth of the clusters and precipitates of the alloys during pure ageing, including both natural and artificial ageing, shares similar trends, where a large growth rate occurs first and then the rate decreases with the ageing time [11, 22, 23]. Hence, the evolution of the new precipitate radius (r_n) during both natural and artificial ageing can be empirically represented by Eq. (3) without the dislocation related term, as:

$$\dot{\bar{r}}_n = C_r(Q - \bar{r}_n)^{m_1} \tag{13}$$

where $\bar{r}_n = r_n/r_{nc}$ is the normalised radius of the new precipitates and r_{nc} represents the corresponding critical value (peak-aged value for artificial ageing and saturate value for natural ageing). C_r is a temperature-dependant material constant. Q represents the normalised saturate radius of the new precipitates during ageing and it is 1 during natural ageing.

During natural ageing, where the as-quenched alloys are aged to T3 or T4 tempers at room temperature, the precipitates ($\bar{r}_{n1}$) are much less developed than the peak-aged ones in artificial ageing, and their contributions to the yield strength of the alloys (σ_{n1}), can be directly modelled by the shearing mechanism, as [7]:

$$\dot{\sigma}_{n1} = C_A \bar{r}_{n1}^{m_9} \dot{\bar{r}}_{n1} \tag{14}$$

where C_A and m_9 are material constants and $\bar{r}_{n1}$ is the normalised radius of the new naturally-aged precipitates.

During artificial ageing, where the as-quenched alloys are aged to T6 or T8 tempers at an elevated temperature, the strength contribution (σ_{n2}) from the new precipitates ($\bar{r}_{n2}$) can be modelled directly by Eq. (7). Meanwhile, when the alloys being artificially aged is with T3 or T4 initial tempers, an initial reversion of yield strength may occur in some alloys because of the dissolution of the naturally-aged precipitates [24]. The normalised dissolving precipitate radius ($\bar{r}_d$) and its strength contribution (σ_d) during artificial ageing can be directly modelled by Eqs. (4) and (8).

The evolution of the normalised solute concentration ($\bar{c}$) during both natural and artificial ageing can be modelled according to Eq. (5), as:

$$\dot{\bar{c}} = -A_1(\bar{c} - \bar{c}_a) \tag{15}$$

where A_1 is a temperature-dependant material constant to characterise the speed of the solute loss during ageing and is small for natural ageing to represent the slow solute diffusion at room temperature [25]. The corresponding strength contribution (σ_{ss}) can be modelled by Eq. (9).

3. Model implementation for multistep heat-treated aluminium alloys

3.1 Initial and equilibrium internal variables

The overall yield strength of aluminium alloys before ageing or creep-ageing is determined by the strength components from the dislocations (σ_{dis_0}), solid solutes (σ_{ss_0}) and precipitates (σ_{p_0}). These components can be estimated according to the yield strength of the alloys that have undergone particular heat treatments. For the as-quenched and naturally-aged (T3/T4) alloys, their initial solid solution component (σ_{ss_0}) can be approximated by the yield strength of the corresponding solution heat-treated alloys. While for the peak-aged alloys (T6/T8), in which significant solute loss had occurred during artificial ageing, the initial value can be estimated according to the equilibrium solute concentration at the age temperature ($\bar{c}_a$), as

$\sigma_{ss_0} \times \bar{c}_a^{\,2/3}$ [26]. The initial strength contribution from dislocations (σ_{dis_0}) can be obtained from the yield strength increase of the alloys after pre-stretching. Finally, the initial precipitation strength component (σ_{p_0}) can be estimated according to σ_{ss_0} and σ_{dis_0} using Eq. (11). The detailed estimation processes for these initial strength components of the alloys with general temper conditions, including as-quenched, T3/T4 and T6/T8, are illustrated in Fig. 1 and listed in Table 1. In addition, the initial creep threshold stress (σ_{th_0}) of the alloys before creep-ageing can be determined by the power-law creep equation [27], which will be shown later in Section 4.

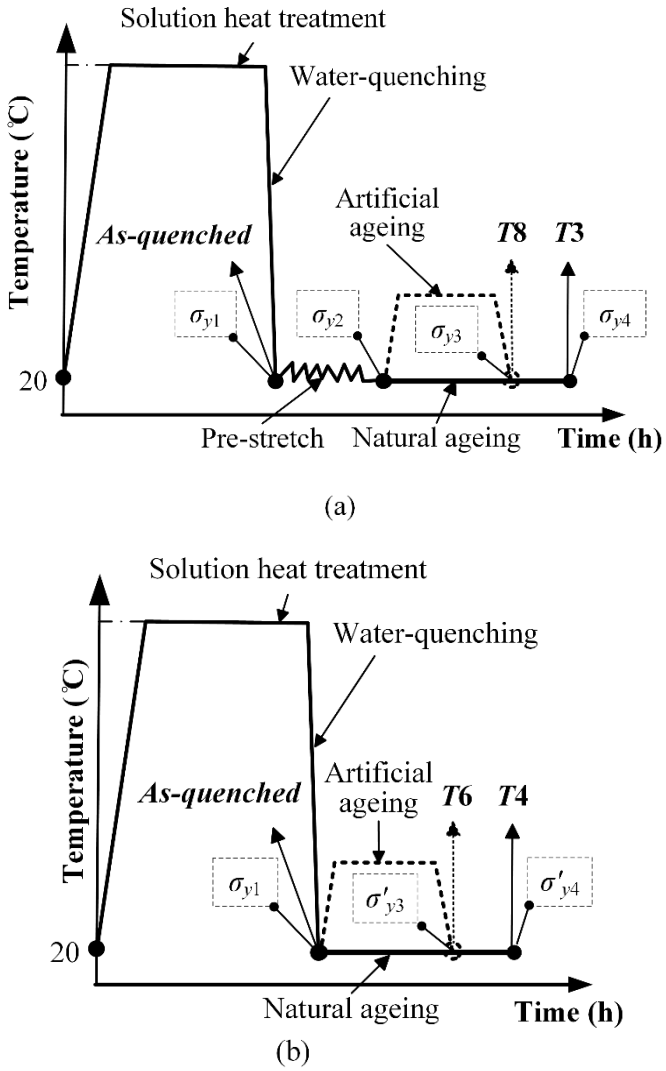


Figure 1. Schematics of heat treatments and corresponding yield strength data for the as-quenched, T3/T8 and T4/T6 tempers: (a) with pre-stretch and (b) without pre-stretch.

Table 1. Determination of initial strength components with various initial tempers.

Initial temper	Solid solution strength component (σ_{ss_0})	Dislocation strength component (σ_{dis_0})	Precipitation strength component (σ_{p_0})
As-quenched	σ_{y1}	0	0
T3	σ_{y1}	$\sigma_{y2}-\sigma_{y1}$	$\sqrt{(\sigma_{y4}-\sigma_{ss_0})^2-\sigma_{dis_0}^2}$
T4	σ_{y1}	0	$\sigma'_{y4}-\sigma_{ss_0}$
T6	$\sigma_{y1}\times\bar{c}_a{}^{2/3}$	0	$\sigma'_{y3}-\sigma_{ss_0}$
T8	$\sigma_{y1}\times\bar{c}_a{}^{2/3}$	$\sigma_{y2}-\sigma_{y1}$	$\sqrt{(\sigma_{y3}-\sigma_{ss_0})^2-\sigma_{dis_0}^2}$

The equilibrium solute concentration of an aluminium alloy at the ageing temperature T_a can be calculated by the following equation [26]:

$$c_a = A_0 \exp\left(-\frac{Q_s}{RT_a}\right) \tag{16}$$

where A_0 is a material constant and Q_s is the free energy of solution of the alloy. The normalised equilibrium value ($\bar{c}_a$) can be obtained from [21]:

$$\bar{c}_a = \frac{c_a}{c_s} = \exp\left(\frac{Q_s}{R}\left(\frac{1}{T_s}-\frac{1}{T_a}\right)\right) \tag{17}$$

where c_s is the equilibrium solute concentration at the SHT temperature T_s.

The initial value of the normalised solute concentration ($\bar{c}_0$) is 1 for the as-quenched alloy and should be less than 1 after natural or artificial ageing. When the alloy is naturally or artificially aged, $\bar{c}_0$ for the subsequent heat treatments can be related to the corresponding normalised precipitate radius ($\bar{r}$) [8]:

$$\bar{c}_0 = 1-\alpha\bar{r}^3 \tag{18}$$

where α is a coefficient. The coefficient α can be calculated according to the critical value of $\bar{r}_{n2c}$=1 and $\bar{c}_a$ as $\alpha = 1-\bar{c}_a$.

The critical values for the normalised precipitate radii $\bar{r}_{n1}$, $\bar{r}_d$ and $\bar{r}_{n2}$ are 1, however the corresponding normalised solute concentration are different. In order to unify their different levels of contributions to the solute loss, the artificially aged new precipitate radius ($\bar{r}_{n2}$) is considered as a standard normalised value throughout the multistep heat treatments, and $\bar{r}_{n1}$ or $\bar{r}_d$ is adjusted to be equivalent to the standard value by a factor $\beta^{1/2}$, which was also used in Eq. (2) to unify the particular contributions to the creep strain rate evolution from $\bar{r}_d$ and $\bar{r}_{n2}$. Hence, after natural ageing, the initial normalised solute concentration can be calculated according to Eq. (18), as $\bar{c}_0 = 1-\alpha(\beta^{1/2}\bar{r}_{n1})^3$. On the other hand, after artificial ageing, the initial normalised solute concentration is $\bar{c}_0 = 1-\alpha(\bar{r}_{n2}+\beta^{1/2}\bar{r}_d)^3$.

The coefficient β can be estimated according to the strength contributions from different precipitate types at their critical states [21], as:

$$\frac{\sigma_{im}}{\sigma_{n2m}} = \left(\frac{\beta^{1/2}\bar{r}_{ic}}{\bar{r}_{n2c}}\right)^2 = \beta \tag{19}$$

where $\bar{r}_{ic}$ represents the critical value of $\bar{r}_{n1c}$ or $\bar{r}_{dc}$ and both $\bar{r}_{ic}$ and $\bar{r}_{n2c}$ are 1. The corresponding maximum strength contributions, σ_{im} and σ_{n2m}, can be obtained by the yield strength curve of the alloy during the ageing processes, as depicted in an earlier study [21].

3.2 Determination of material constants in the model

As the constitutive model used in this study consists of non-linear ordinary differential equations and cannot be solved analytically, a multi-step fitting process as detailed in earlier studies [19, 21] was used to determine and optimise the material constants in the models for natural ageing, artificial ageing and creep-ageing. In this process, a numerical optimisation technique was used so as to achieve the minimum sum of the square of errors between the experimental and numerical results. The objective function used in the numerical optimisation process is defined as [28]:

$$f(x) = \sum_{j=1}^{n_1}\sum_{i=1}^{m_j} w_{ij}\left(O_{ij}^{c} - O_{ij}^{e}\right)^2 \tag{20}$$

where $x = (x_1, x_2, \ldots, x_s)$ represents all material constants need to be optimised and w_{ij} is a weighting function. n_1 represents the number of experimental curves, m_j is the number of data points for the *j*th experimental curve. w_{ij} is a weighting function. $(O_{ij}^{c} - O_{ij}^{e})$ is the difference between the numerical and experimental data at the same processing time. *O* represents the yield strength data for ageing heat treatments, while for the creep-ageing condition, *O* is the creep strain data. The final error between the experiments and numerical models with the determined constants is estimated by their root-mean-square deviation (RMSD) and has been provided for each case in Section 4.

For the creep-ageing condition where multiple sets of experimental data under different stress levels were available, only three sets of the data were employed for the determination of the material constants, the other sets of experimental data were used to verify the effectiveness of the determined material constants.

4. Model applications and discussion

In this section, the model presented in Section 2 is applied to some heat treatment processes whose data can be obtained from literature. The cases studied include natural ageing with simple and complex hardening behaviour, artificial ageing of as-quenched and T3 temper with complex precipitation behaviour, creep-ageing with as-quenched, naturally aged and artificially aged conditions.

4.1 Natural ageing

Natural ageing of two typical aluminium alloys, which demonstrate either simple or complex precipitation behaviour, was modelled by the following set of equations summarised from Section 2:

$$\begin{cases} \dot{\bar{r}}_{n1} = C_r(1-\bar{r}_{n1})^{m_1} \\ \dot{\bar{c}} = -A_1(\bar{c}-\bar{c}_a) \\ \dot{\sigma}_{n1} = C_A \bar{r}_{n1}^{m_9} \dot{\bar{r}}_{n1} \\ \dot{\sigma}_{ss} = -C_{ss}|\dot{\bar{c}}|^{m_5}(\bar{c}-\bar{c}_a) \\ \sigma_y = \sigma_{ss} + \sigma_{n1} \end{cases} \quad (21)$$

The first case is for natural ageing of an as-quenched Al-4Cu-0.3Mg-0.4Ag alloy with a single-peak hardness curve. The hardness evolution during natural ageing of the alloy was reported in [14]. In this case, the initial normalised radius of precipitates of this as-quenched alloy ($\bar{r}_{n1_0}$) was 0 and the initial solute concentration value ($\bar{c}_0$) was 1 before natural ageing. Their initial strength contributions (σ_{n1_0} and σ_{ss_0}) were obtained according to Table 1. The most commonly used relationship between the yield strength and hardness, $\sigma = 3 * HV$ [29], was applied in this study to demonstrate the capability of the constitutive model in predicting the strengthening of the alloys during ageing heat treatment. Some experiments on true yield strength would best be carried out to calibrate the model before it is used for guiding the ageing practice. All initial values are listed in Table 2. The equilibrium state of the solute concentration ($\bar{c}_a$) was calculated according to Eq. (17) with Q_s = 25 kJ mol^{-1} [7]. At room temperature (T_a=293 K), solute diffusion was very slow and therefore the temperature-dependent material constant A_1 was small. Other material constants were determined according to Section 3.2 and presented in Table 2.

Table 2. Initial and equilibrium values and material constants for natural ageing of the as-quenched Al-4Cu-0.3Mg alloy.

Initial and equilibrium values	$\bar{r}_{n1_0}$ (-)	$\bar{c}_0$ (-)	σ_{n1_0} (MPa)	σ_{ss_0} (MPa)	$\bar{c}_a$ (-)		
	0	1	0	219	0.0132		
Material constants	C_r (h^{-1})	m_1 (-)	C_A (MPa)	m_9 (-)	A_1 (-)	C_{ss} (MPa)	m_5 (-)
	5E-2	1.2	90	0.05	1e-6	15	0.7

The predicted results from the determined material constants were compared with experimental data [14] in Fig. 2. Good agreement was achieved where the root-mean-square deviation (RMSD) between corresponding modelling and experimental hardness data is only 1.8 VHN, demonstrating the effectiveness of the current model for the application to natural ageing with simple hardening behaviour.

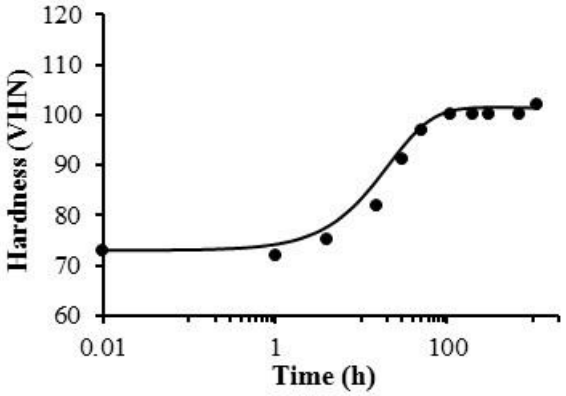


Figure 2. Hardness evolution during natural ageing of as-quenched Al-4Cu-0.3Mg alloy from experiments (symbols) [14] and age hardening model (solid line).

Some aluminium alloys have a more complex hardening behaviour during natural ageing. Ringer et al. [14] reported detailed data for natural ageing of an Al-5.3Cu-1.3Li alloy with or without pre-stretch (T3 and T4 temper). Different from the Al-Cu-Mg alloy shown above, more complex yield strength evolution curves with a shoulder and a peak were observed for both temper conditions because of the different growth progresses of the GP zones and δ' precipitates during natural ageing [14]. The initial values of microstructural variables and strength components of the alloy were determined according to Section 3.1 and listed in Table 3. The equilibrium solute concentration ($\bar{c}_a$) was calculated according to a general format of Eq. (17) ($\ln C_a$ = 4.176-9180/RT) for Al-Li alloys [30]. In this case, the evolution of dislocations was ignored during natural ageing and the initial strength contribution from pre-stretch was treated as part of the initial solution hardening component for simplification.

For natural ageing to T3 temper, if Eq. (21) was used directly, where all precipitates were treated as a general type during natural ageing, the computed results (dashed line in Fig. 3) according to the optimised material constants (Table 3) showed apparent discrepancies with the experimental data [14], especially in the first 70 hours.

This is due to the different growth progresses of the GP zones and δ' precipitates during the ageing process [14]. In order to accurately predict the hardening behaviour, microstructural evolutions of the GP zones and δ' precipitates of the alloy were modelled separately during natural ageing. Hence, the equations related to precipitates in Eq. (21) were extended to two sets: one set represented the evolution of GP zones ($\bar{r}_{n1_GP}$ and σ_{n1_GP}) and the other was for δ' ($\bar{r}_{n1_\delta'}$ and $\sigma_{n1_\delta'}$). Their total strength contribution was determined using $\sigma_{n1} = \sqrt{(\sigma_{n1_GP})^2 + (\sigma_{n1_\delta'})^2}$. These two sets of equations were calibrated based on the particular properties of the yield strength curve, where the shoulder of the curve was mainly contributed by the growth of GP zones and the peak was controlled by δ' [14]. The related material constants for these two precipitates were listed in Table 3. The predicted results from the extended model were shown in Fig. 3 with solid line, demonstrating much better agreement with the experimental data through the whole natural ageing period (RMSD = 1.2 VHN) than the original single precipitate type model (dashed line, RMSD = 5.2 VHN). The results indicate

that the current model can be extended to separately model the precipitates which experience different evolution progresses during ageing, and predict complex hardening evolution during natural ageing. It also emphasises the importance of understanding the microstructural evolution and related mechanisms for a good model.

Table 3. Initial and equilibrium values and material constants for natural ageing of pre-stretched Al-Al-5.3Cu-1.3Li alloy.

Initial and equilibrium values	$\bar{r}_{n1_0}$ (-)	$\bar{c}_0$ (-)	σ_{n1_0} (MPa)	σ_{ss_0} (MPa)	$\bar{c}_a$ (-)			
	0	1	0	342	0.11			
Material constants with single precipitate type	C_r (h^{-1})	m_1 (-)	C_A (MPa)	m_9 (-)		A_1 (-)	C_{ss} (MPa)	m_5 (-)
	2E-2	1.2	95	0.64		2e-7	15	0.7
Material constants with double precipitate type	GP zones				δ'			
	C_r (h^{-1})	m_1 (-)	C_A (MPa)	m_9 (-)	C_r (h^{-1})	m_1 (-)	C_A (MPa)	m_9 (-)
	4E-1	1.2	50	0.45	8E-3	1.2	75	0.56

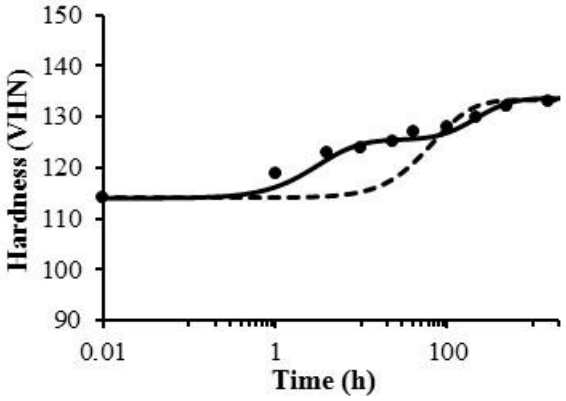


Figure 3. Comparison of hardness evolution during natural ageing of pre-stretched Al-5.3Cu-1.3Li alloy from experiments (symbols) [14] and models with single (dashed line) and double (solid line) precipitate type.

During natural ageing, the same Al-5.3Cu-1.3Li alloy without pre-stretch showed a yield strength behaviour similar to the one with pre-stretch and hence, the extended model with the double precipitate type (GP zones and δ') were used to simulate the ageing process. The initial and equilibrium values of the alloy, as well as the optimised material constants are listed in Table 4. The experimental and model simulation results for the hardness evolution are compared in Fig. 4. It demonstrates the very good simulation results for the complex hardening curve of the material for T4 temper with a RMSD value of 1.3 VHN. Together with the results

shown in Fig. 3, the extended model is shown to be effective in predicting natural ageing of alloys with complex hardening curves.

Table 4. Initial and equilibrium values and material constants for natural ageing of as-quenched Al-5.3Cu-1.3Li alloy.

Initial and equilibrium values	$\bar{r}_{n1_0}$ (-)	$\bar{c}_0$ (-)	σ_{n1_0} (MPa)	σ_{ss_0} (MPa)	$\bar{c}_a$ (-)			
	0	1	0	258	0.11			
Material constants	A_1 (-)	C_{ss} (MPa)	m_5 (-)					
	1e-6	15	0.7					
	GP zones				δ'			
	C_r (h^{-1})	m_1 (-)	C_A (MPa)	m_9 (-)	C_r (h^{-1})	m_1 (-)	C_A (MPa)	m_9 (-)
	4.4E-1	1.2	170	0.51	6E-3	1.2	210	0.69

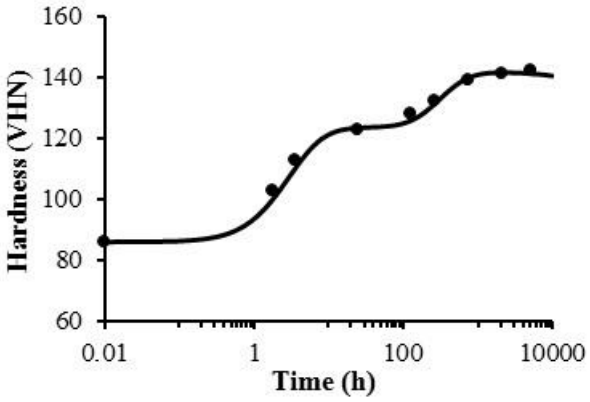


Figure 4. Hardness evolution during natural ageing of as-quenched Al-5.3Cu-1.3Li alloy from experiments (symbols) [14] and double precipitate type model (solid line).

4.2 Artificial ageing

In this section, the model is extended to artificial ageing of some typical Al-Cu-Li alloys with different initial tempers which show complex precipitation progress with more than one main strengthening phases. The following set of equations was used in this case study:

$$\begin{cases} \dot{\bar{r}}_{n2} = C_r(Q - \bar{r}_{n2})^{m_1} \\ \dot{\bar{r}}_d = -C_{r1}/\bar{r}_d \\ \dot{\bar{c}} = -A_1(\bar{c} - \bar{c}_a) \\ \dot{\sigma}_{n2} = C_a \dot{\bar{r}}_{n2}^{m_2}(1 - \bar{r}_{n2}^{m_3}) \\ \dot{\sigma}_d = C_{a1}\bar{r}_d^{m_4}\dot{\bar{r}}_d \\ \dot{\sigma}_{ss} = -C_{ss}|\dot{\bar{c}}|^{m_5}(\bar{c} - \bar{c}_a) \\ \sigma_y = \sigma_{ss} + \sqrt{\sigma_{n2}^2 + \sigma_d^2} \end{cases} \quad (22)$$

Artificial ageing of an as-quenched Al-5.3Cu-1.3Li alloy at 433 K was investigated by Ringer et al. [14] and detailed data on hardness evolution were reported, as shown in Fig. 5 (symbols). During artificial ageing, two types of precipitates (θ' and T_1) appeared in the alloy. θ' precipitates were believed to control the strengthening in the early stage and T_1 precipitates played a more important role in the later stage. The initial variable values of the as-quenched alloy were the same as those listed in Table 3 but $\bar{c}_a$ was updated as the temperature was 433 K, which are presented in Table 5. As no naturally-aged precipitates ($\bar{r}_{n1}$) existed in the alloy before artificial ageing, only new precipitates ($\bar{r}_{n2}$) were considered. Similar with natural ageing of the Al-Cu-Li alloys above, the extended model with the double precipitate type (θ' and T_1) was evaluated. The related material constants are presented in Tables 5. Fig. 5 compares the predicted results with the experimental data and very good agreement can be observed (RMSD = 3.8 VHN), showing the effectiveness of the extended model in predicting artificial ageing of aluminium alloys with complex hardening curves.

Table 5. Initial and equilibrium values and material constants for artificial ageing of as-quenched Al-5.3Cu-1.3Li alloy.

Initial and equilibrium values	$\bar{r}_{n2_0}$ (-)	$\bar{c}_0$ (-)	σ_{n2_0} (MPa)	σ_{ss_0} (MPa)	$\bar{c}_a$ (-)					
	0	1	0	258	0.324					
Material constants	A_1 (-)	C_{ss} (MPa)	m_5 (-)	Q (-)						
	0.02	60	0.48	1.03						
			θ'					T_1		
	C_r (h^{-1})	m_1 (-)	C_a (MPa)	m_2 (-)	m_3 (-)	C_r (h^{-1})	m_1 (-)	C_a (MPa)	m_2 (-)	m_3 (-)
	1.2	1.2	200	0.9	1.05	3.4E-2	0.73	56	0.38	1.5

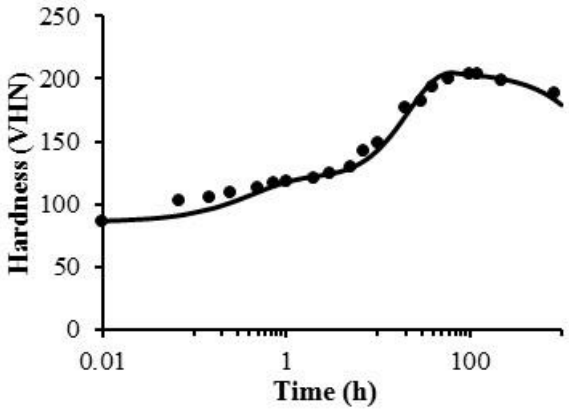


Figure 5. Hardness evolution during artificial ageing of as-quenched Al-5.3Cu-1.3Li alloy from experiments (symbols) [14] and double precipitate type model (solid line).

Kumar et al. [24] investigated microstructural evolution and hardness responses during artificial ageing of a naturally-aged Al-5.4Cu-1.6Li alloy (T3 temper) at 433 K. T_1 precipitates were reported to be the main strengthening phase in the alloy during artificial ageing [24]. Therefore a general precipitate type was used to represent the new precipitates. For this T3 material, the initial normalised radius of the new precipitates ($\bar{r}_{n2_0}$) was 0 and the initial value of the dissolving precipitates ($\bar{r}_{d_0}$) was 1. The normalised equilibrium solute concentration ($\bar{c}_a$) was 0.324 at 433 K. The initial solute concentration value ($\bar{c}_0$) was calculated using Eq. (18). β was obtained from Eq. (19), where σ_{n2} = 86 MPa and σ_d = 16 MPa from the harness curve in Fig. 6. As a result, β = 0.186 and $\bar{c}_0$ = 0.95. All the initial values of the internal variables and the determined material constants are listed in Table 6. Comparing the predicted hardness evolution results with experiments in Fig. 6, it can be seen that good agreement has been achieved (RMSD = 2.8 VHN).

Table 6. Initial and equilibrium values and material constants for artificial ageing of Al-Cu-Li alloy with T3 initial temper.

$\bar{r}_{n2_0}$ (-)	$\bar{r}_{d_0}$ (-)	$\bar{c}_0$ (-)	σ_{n2_0} (MPa)	σ_{d_0} (MPa)	σ_{ss_0} (MPa)	$\bar{c}_a$ (-)	β (-)
0	1	0.95	0	16	184.4	0.324	0.186

C_r (h^{-1})	Q (-)	m_1 (-)	C_a (MPa)	m_2 (-)	m_3 (-)	C_{r1} (h^{-1})	C_{a1} (MPa)	m_4 (-)	A_1 (-)	C_{ss} (MPa)	m_5 (-)
3.8E-2	1.03	0.8	9.5	0.15	1.0	0.95	23	0.5	0.07	40	0.85

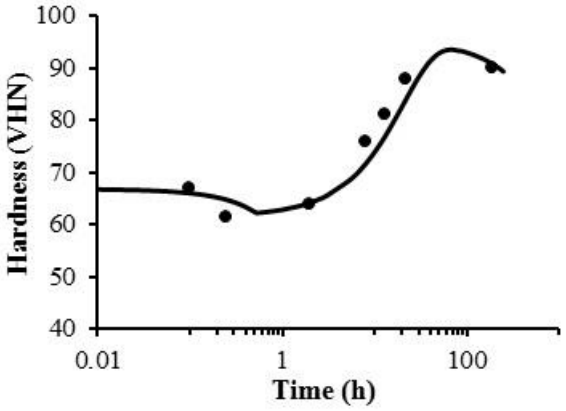


Figure 6. Hardness evolution during artificial ageing of T3 tempered Al-Cu-Li alloy from experiments (symbols) [24] and age hardening model (solid line)

In summary, the above results for both Al-Cu-Mg and Al-Cu-Li alloys verify that the age hardening model proposed in this study can be used to predict both the simple and complex evolutions of microstructures and yield strength during natural and artificial ageing of various multistep heat-treated aluminium alloys. It is shown that it is very important to understand the microstructural evolution and its effect on strength evolution, and hence to choose a proper model that can closely represent the experimental results.

4.3 Creep-ageing of multistep heat-treated aluminium alloys

In this section, the constitutive model was applied to CAF of some typical multistep heat-treated 7xxx and 2xxx aluminium alloys with different initial temper conditions, using the following set of equations [21]:

$$\begin{cases} \dot{\varepsilon}_{cr} = A_4 sinh\{B_1(\sigma - \sigma_{th_0})(1-H)\} sign(\sigma) \\ H = k_1\bar{\rho} + k_2\bar{c} + k_3(\bar{r}_{n2} + \beta^{1/2}\bar{r}_d) \\ \dot{\bar{r}}_{n2} = C_r(Q - \bar{r}_{n2})^{m_1}(1 + \gamma_0\bar{\rho}^{m_8}) \\ \dot{\bar{r}}_d = -C_{r1}/\bar{r}_d \\ \dot{\bar{c}} = -A_1(\bar{c} - \bar{c}_a)(1 + \gamma_0\bar{\rho}^{m_8}) \\ \dot{\bar{\rho}} = A_2(1-\bar{\rho})|\dot{\varepsilon}_{cr}|^{m_6} - C_p\bar{\rho}^{m_7} \\ \dot{\sigma}_{n2} = C_a\dot{\bar{r}}_{n2}^{m_2}(1 - \bar{r}_{n2}^{m_3}) \\ \dot{\sigma}_d = C_{a1}\bar{r}_d^{m_4}\dot{\bar{r}}_d \\ \dot{\sigma}_{ss} = -C_{ss}|\dot{\bar{c}}|^{m_5}(\bar{c} - \bar{c}_a) \\ \dot{\sigma}_{dis} = A_3 n\bar{\rho}^{n-1}\dot{\bar{\rho}} \\ \sigma_y = \sigma_{ss} + \sqrt{\sigma_{n2}^2 + \sigma_d^2 + \sigma_{dis}^2} \end{cases} \quad (23)$$

(a) Creep-ageing of as-quenched Al-Zn-Mg alloy

Creep-ageing of an as-quenched AA7055 at 393 K was investigated by Zhan et al. [19]. Only new precipitates ($\bar{r}_{n2}$) could be observed during creep-ageing of the as-quenched alloys. The

initial values of the microstructures and strength components are listed in Table 7, where the initial normalised dislocation density was negligible and was set as 1E-6. $\bar{c}_a$ was calculated according to Eq. (17), where Q_s = 8.9 KJmol^{-1} [10]. The initial creep threshold stress of the as-quenched alloy was assumed insignificant and was set to 0 MPa [27]. The creep curves of the alloy exhibited the conventional two-stage behaviour, which was widely explained by dislocation and precipitation hardening. Hence, the creep strain rate of the alloy was mainly determined by the normalised dislocation density ($\bar{\rho}$) and normalised precipitate radius ($\bar{r}_{n2}$). Table 7 lists the material constants optimised according to Section 3.2.

Table 7. Initial and equilibrium values and material constants for creep-ageing of as-quenched AA7055 at 393 K.

$\bar{\rho}_0$	$\bar{c}_0$	$\bar{r}_{n2_0}$	σ_{n2_0}	σ_{ss_0}	σ_{dis_0}	$\bar{c}_a$	σ_{th_0}	C_r	Q
(-)	(-)	(-)	(MPa)	(MPa)	(MPa)	(-)	(MPa)	(h^{-1})	(-)
1E-6	1	0	0	387	0	0.27	0	3.1E-2	1.69
m_1	C_a	m_2	m_3	A_1	C_{ss}	m_5	A_2	m_6	m_7
(-)	(MPa)	(-)	(-)	(-)	(MPa)	(-)	(h^{-1})	(-)	(-)
1.3	124.3	0.45	0.75	0.09	80	0.34	380	0.9	1.3
C_p	A_3	n	A_4	B_1	k_1	k_2	k_3	γ_0	m_8
(-)	(-)	(-)	(-)	(-)	(-)	(-)	(-)	(-)	(-)
0.07	181.5	0.8	3E-5	1.9E-2	0.45	0.05	0.25	2.0	1.98

The experimental results under stress levels of 190.0, 252.2 and 308.9 MPa were used for material constants determination and the effectiveness of the fitted equations were verified by comparing the predicted data and experimental data under other stress levels (dashed lines in Fig. 8). The predicted yield strength curves during creep-ageing under different stress levels are plotted and compared with the experiments in Fig. 7. The modelling results correspond well with experiments and both illustrate an accelerating age hardening behaviour with increasing applied stress. The creep strain curves under four applied stress levels are shown in Fig. 8, where modelling results show good agreement with the experiments under all stress levels (the RMSD values for the strain data under stress levels of 190.0, 252.2, 308.9 and 357.8 MPa are respectively 0.015%, 0.02%, 0.015% and 0.033%), demonstrating the effectiveness of the constitutive model in predicting creep-ageing behaviour of the as-quenched alloys.

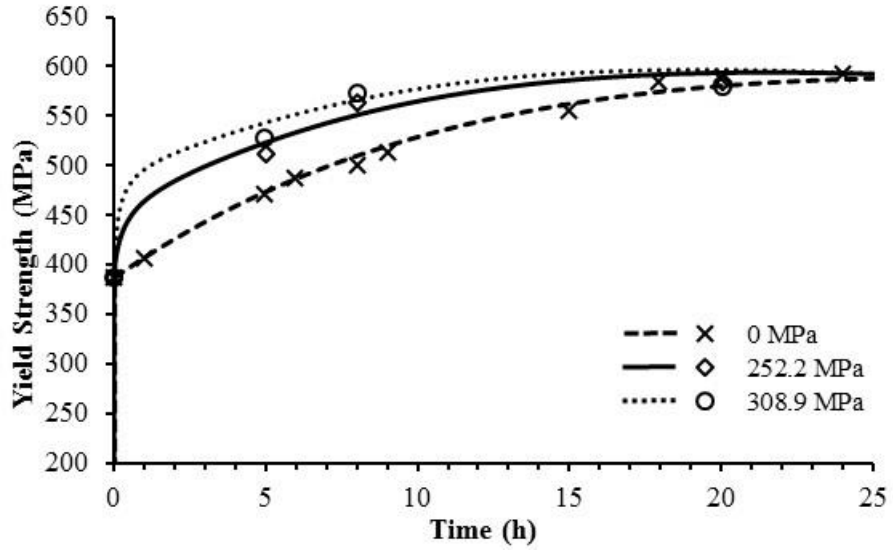


Figure 7. Comparison of yield strength evolution under different stress levels during creep-ageing of as-quenched AA7055 at 393 K between experiments (symbols) [19] and models (lines).

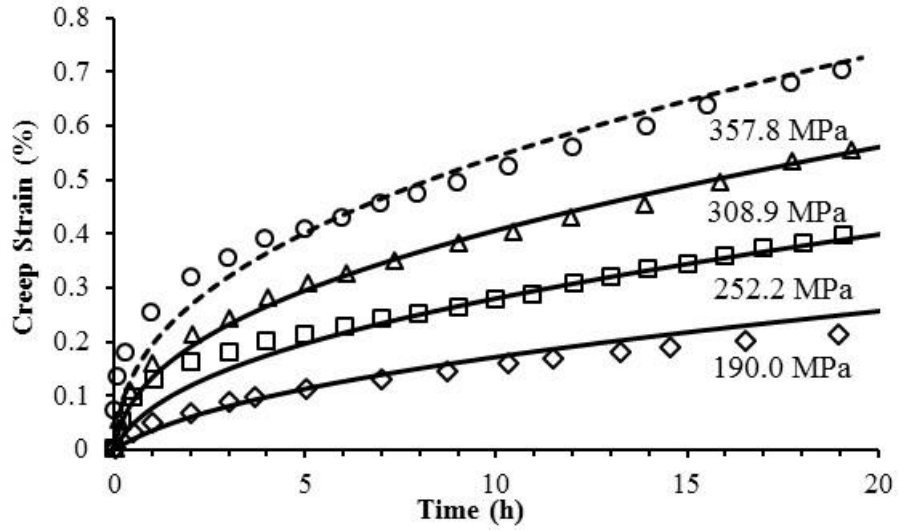


Figure 8. Comparison of creep strain curves under different stress levels during creep-ageing of as-quenched AA7055 at 393 K between experiments (symbols) [19] and models (solid lines for material constants determination and dashed line for verification).

(b) Creep-ageing of naturally-aged Al-Cu-Li alloy

A new double primary creep feature and a yield strength evolution with an initial reversion were observed during creep-ageing of AA2050-T34 [6]. For this alloy, both dissolving and new precipitates have effects on hardening and creep behaviour and need be considered in the creep-ageing model. The procedures to obtain the initial and equilibrium values followed those detailed in Section 3, and the resultant values are listed in Table 8 [21]. The material constants were determined using the experimental data under stress levels of 150, 162.5 and 175 MPa and the optimised material constants are also presented in Table 8. These determined constants were used to predict the results under other stress levels (dashed lines in Fig. 10). Figs. 9 and

10 compare the modelling and experimental results of the yield strength and creep curves under different stress levels, both showing very good agreement between each other (the RMSD values for the strain data under stress levels of 100, 150, 162.5, 175 and 187.5 MPa in Fig. 10 are 0.0022%, 0.0019%, 0.0015%, 0.0026% and 0.0018% respectively), and again indicating the effectiveness of the model in predicting the creep-ageing behaviour of the alloys with T3 temper.

Table 8. Initial and equilibrium values and material constants for creep-ageing of AA2050-T34 at 428 K.

$\bar{\rho}_0$	$\bar{c}_0$	$\bar{r}_{d_0}$	$\bar{r}_{n2_0}$	β	σ_{d_0}	σ_{n2_0}	σ_{ss_0}	σ_{dis_0}
(-)	(-)	(-)	(-)	(-)	(MPa)	(MPa)	(MPa)	(MPa)
1E-6	0.978	1	0	0.101	110	0	120	100
$\bar{c}_a$	C_r	Q	m_1	C_a	m_2	m_3	C_{r1}	C_{a1}
(-)	(h^{-1})	(-)	(-)	(MPa)	(-)	(-)	(h^{-1})	(MPa)
0.316	0.108	1.1	1.25	180	0.65	6.5	0.108	120
m_4	A_1	C_{ss}	m_5	A_2	m_6	m_7	C_p	A_3
(-)	(-)	(MPa)	(-)	(h^{-1})	(-)	(-)	(-)	(-)
0.10	0.45	40.0	0.02	1.7	0.03	2.1	0.07	12
n	A_4	B_1	k_1	k_2	k_3	γ_0	m_8	σ_{th_0}
(-)	(-)	(-)	(-)	(-)	(-)	(-)	(-)	(MPa)
0.8	4.5E-4	1.32E-2	0.618	0.622	0.226	0.08	1.28	18

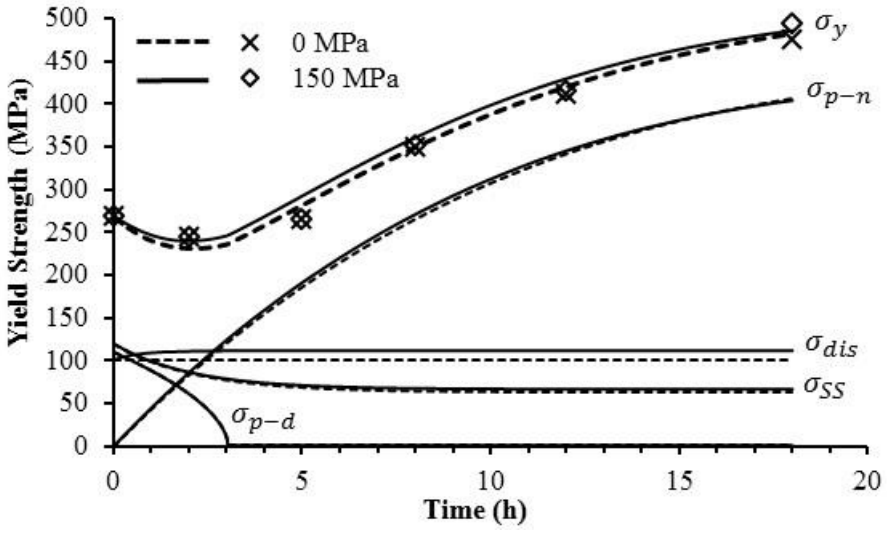


Figure 9. Comparison of yield strength evolution under different stress levels during creep-ageing of AA2050-T34 at 428 K between experiments (symbols) [6] and models (lines).

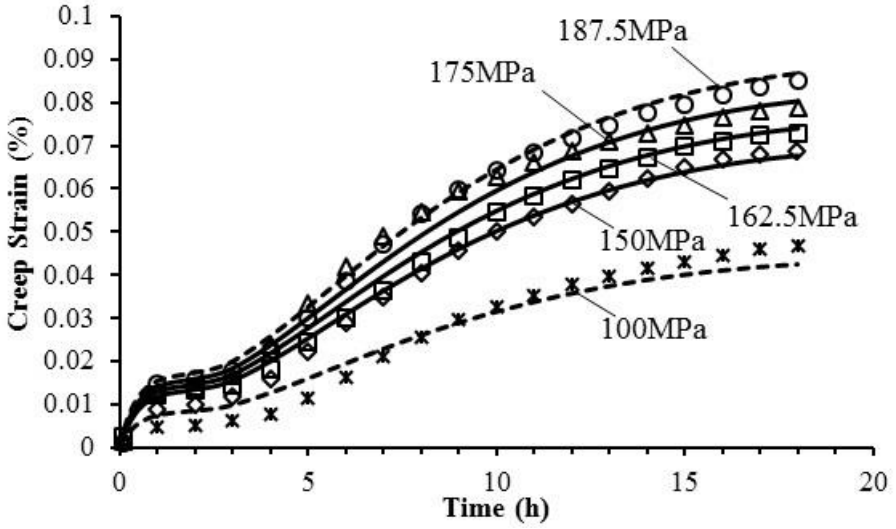


Figure 10. Comparison of creep strain curves under different stress levels during creep-ageing of AA2050-T34 at 428 K between experiments (symbols) [31] and models (solid lines for material constants determination and dashed lines for verification).

(c) Creep-ageing of peak-aged Al-Zn-Mg alloy

Finally, the constitutive model was applied to creep-ageing of a peak-aged Al-Zn-Mg alloy (AA7050). Yang et al. [20] investigated creep-ageing behaviour of the alloy at 447 K. The alloy was peak-aged, its solute concentration had already reached an equilibrium state and would be stable in the subsequent CAF process. Thus $\bar{c}_0 = \bar{c}_a$ and the changes in $\bar{c}$ and σ_{ss} are negligible. Only the artificially-aged precipitates exist in the alloy during the CAF process, which already reached its critical value and hence $\bar{r}_{n2_0} = 1$. The initial strength components of the alloy were referenced from [20]. As mentioned in Section 3.1, σ_{th_0} can be determined by using the power-law creep equation $\dot{\varepsilon}_{cr} = A(\sigma - \sigma_{th})^n$, where A can be treated as a constant and the index n is generally set as 4 for aluminium alloys [27]. Hence, the threshold stress (σ_{th_0}) of the alloy can be determined from the linear plot of $\dot{\varepsilon}_{cr}^{1/n}$ versus σ, where $\dot{\varepsilon}_{cr}$ is the creep strain rate at the steady-state creep stage and σ is the applied stress. σ_{th_0} = 43 MPa was then obtained according to the data from [20]. The *ln-ln* plot of the creep strain rate ($\dot{\varepsilon}_{cr}$) versus the applied effective stress ($\sigma - \sigma_{th_0}$) is shown in Fig. 11 with σ_{th_0} = 43 MPa, a good linear relationship between them was observed, indicating the validity of the estimation of σ_{th_0}. All initial and equilibrium values, as well as the optimised material constants are listed in Table 9.

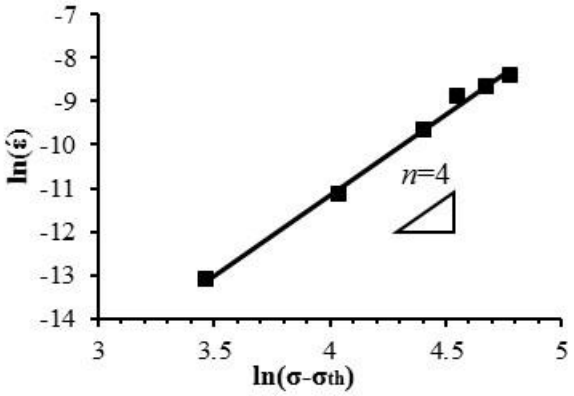


Figure 11. *ln-ln* plot of creep strain rate ($\dot{\varepsilon}_{cr}$) versus the effective applied stress ($\sigma - \sigma_{th_0}$) (σ_{th_0} = 43 MPa) for CAF of peak-aged AA7050 at 447 K.

Table 9. Initial and equilibrium values and material constants for creep-ageing of peak-aged AA7050 at 447 K.

$\bar{\rho}_0$	$\bar{c}_0$	$\bar{r}_{n2_0}$	σ_{n2_0}	σ_{ss_0}	σ_{dis_0}	$\bar{c}_a$	σ_{th_0}	C_r	Q
(-)	(-)	(-)	(MPa)	(MPa)	(MPa)	(-)	(MPa)	(h^{-1})	(-)
1E-6	0.27	1	273.4	300	0	0.27	43	0.31	2.69
m_1	C_a	m_2	m_3	A_1	C_{ss}	m_5	A_2	m_6	m_7
(-)	(MPa)	(-)	(-)	(-)	(MPa)	(-)	(h^{-1})	(-)	(-)
1.3	61.5	0.52	0.65	0	0	0	480	0.9	1.3
C_p	A_3	n	A_4	B_1	k_1	k_2	k_3	γ_0	m_8
(-)	(-)	(-)	(-)	(-)	(-)	(-)	(-)	(-)	(-)
0.07	21.5	0.8	1.6E-5	4.34E-2	0.6	0	0.005	2.7	1.98

Both computed and experimental results of the yield strength and creep strain curves under different stress levels during the CAF process of the alloy are shown in Figs. 12 and 13. The material constants were determined by the experimental data under stress levels of 100, 125 and 150 MPa and the others in Fig. 13 were predicted by the determined model (dashed lines). Although slight discrepancies between experiments and models exist in the yield strength curves in Fig. 12, the trend of the curves and their accelerating softening phenomena with increasing applied stress during creep-ageing were well predicted. Meanwhile, the predicted creep strain curves correspond well with experiments under all stress levels (the RMSD values for the strain data are 0.0048%, 0.0055%, 0.0046%, 0.0033% and 0.0049% respectively for stress levels of 75, 100, 125, 150 and 162.5 MPa). Hence, the model can be effectively applied to CAF of aluminium alloys with T6 initial temper.

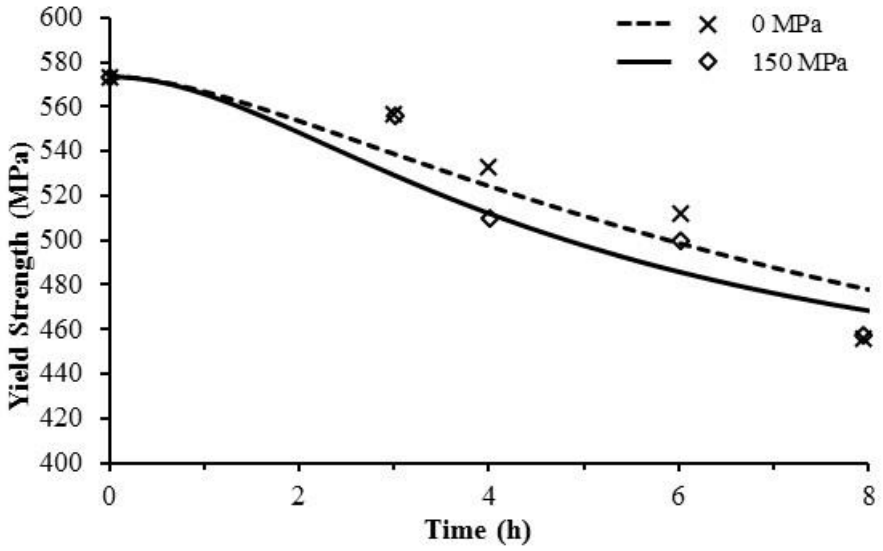


Figure 12. Comparison of yield strength evolution under different stress levels during creep-ageing of peak-aged AA7050 at 447 K between experiments (symbols) [20] and models (lines).

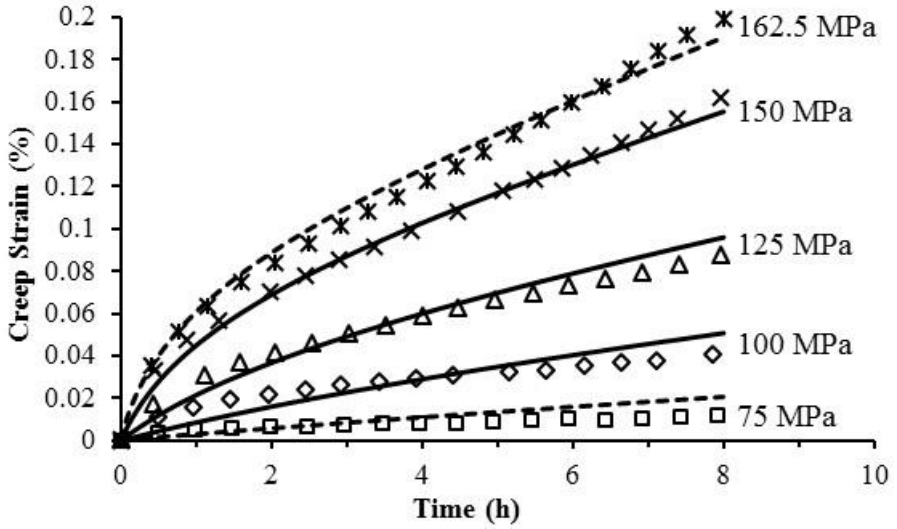


Figure 13. Comparison of creep strain curves under different stress levels during creep-ageing of peak-aged AA7050 at 447 K between experiments (symbols) [20] and models (solid lines for material constants determination and dashed lines for verification).

5. Conclusions

A unified constitutive model developed for creep-ageing of AA2050-T34 has been successfully extended to applications of multistep heat treatments of various aluminium alloys, as well as creep-ageing processes with different initial temper conditions. The internal microstructural variables, namely the precipitate radius, solute concentration and dislocation density were modelled with a unified normalised standard throughout the multistep heat treatments. Together with the methods proposed to determine the initial and equilibrium values of the material variables during multistep heat treatments, the extended model successfully predicted the simple and complex hardening behaviour during natural ageing and artificial

ageing and both strength and creep responses during creep-ageing of aluminium alloys with various initial temper conditions. It is important to understand the microstructural evolution and its effect on strength evolution so that a proper model can be selected for a specific ageing process.

Acknowledgements

The authors are grateful to the financial support from ESI Group (France) (Grant no. MESM_NEI065). Mr Y. Li would also like to thank the support from the China Scholarship Council (CSC) (Grant no. 201406320170).

References:

[1] L. Zhan, J. Lin, T. Dean, A review of the development of creep age forming: experimentation, modelling and applications, International Journal of Machine Tools and Manufacture 51(1) (2011) 1-17.
[2] J. Du, E. El-Magd, Description of the creep behaviour of the precipitation-hardened material Al-Cu-Mg alloy 2024 using finite element computations based on microstructure mechanical models, Computational materials science 7(1) (1996) 200-207.
[3] A.C. Lam, Z. Shi, H. Yang, L. Wan, C.M. Davies, J. Lin, S. Zhou, Creep-age forming AA2219 plates with different stiffener designs and pre-form age conditions: Experimental and finite element studies, Journal of Materials Processing Technology 219 (2015) 155-163.
[4] Y.C. Lin, J.-L. Zhang, G. Liu, Y.-J. Liang, Effects of pre-treatments on aging precipitates and corrosion resistance of a creep-aged Al–Zn–Mg–Cu alloy, Materials & Design 83 (2015) 866-875.
[5] Y.C. Lin, G. Liu, M.-S. Chen, J. Li, M. Zhou, H.-M. Zhou, Effects of two-stage creep-aging processing on mechanical properties of an Al–Cu–Mg alloy, Materials & Design 79 (2015) 127-135.
[6] Y. Li, Z. Shi, J. Lin, Y.-L. Yang, B.-M. Huang, T.-F. Chung, J.-R. Yang, Experimental investigation of tension and compression creep-ageing behaviour of AA2050 with different initial tempers, Materials Science and Engineering: A 657 (2016) 299-308.
[7] H. Shercliff, M. Ashby, A process model for age hardening of aluminium alloys—I. The model, Acta Metallurgica et Materialia 38(10) (1990) 1789-1802.
[8] S. Esmaeili, D. Lloyd, W. Poole, Modeling of precipitation hardening for the naturally aged Al-Mg-Si-Cu alloy AA6111, Acta Materialia 51(12) (2003) 3467-3481.
[9] W. Sha, Application of simple practical models for early stage ageing precipitation kinetics and hardening in aluminium alloys, Materials & Design 28(2) (2007) 528-533.
[10] M. Starink, S. Wang, A model for the yield strength of overaged Al–Zn–Mg–Cu alloys, Acta Materialia 51(17) (2003) 5131-5150.
[11] B. Raeisinia, W. Poole, X. Wang, D. Lloyd, A model for predicting the yield stress of AA6111 after multistep heat treatments, Metallurgical and Materials Transactions A 37(4) (2006) 1183-1190.
[12] Y. Zhao, Z. Yang, Z. Zhang, G. Su, X. Ma, Double-peak age strengthening of cold-worked 2024 aluminum alloy, Acta Materialia 61(5) (2013) 1624-1638.
[13] S.A.J. Jahromi, Creep behavior of spray-cast 7XXX aluminum alloy, Materials & Design 23(2) (2002) 169-172.
[14] S. Ringer, B. Muddle, I. Polmear, Effects of cold work on precipitation in Al-Cu-Mg-(Ag) and Al-Cu-Li-(Mg-Ag) alloys, Metallurgical and Materials Transactions A 26(7) (1995) 1659-1671.

[15] K. Ho, J. Lin, T. Dean, Constitutive modelling of primary creep for age forming an aluminium alloy, Journal of Materials Processing Technology 153 (2004) 122-127.
[16] L.-T. Li, Y. Lin, H.-M. Zhou, Y.-Q. Jiang, Modeling the high-temperature creep behaviors of 7075 and 2124 aluminum alloys by continuum damage mechanics model, Computational Materials Science 73 (2013) 72-78.
[17] Y. Lin, Y.-C. Xia, M.-S. Chen, Y.-Q. Jiang, L.-T. Li, Modeling the creep behavior of 2024-T3 Al alloy, Computational Materials Science 67 (2013) 243-248.
[18] C. Li, M. Wan, X.-D. Wu, L. Huang, Constitutive equations in creep of 7B04 aluminum alloys, Materials Science and Engineering: A 527(16) (2010) 3623-3629.
[19] L. Zhan, J. Lin, T.A. Dean, M. Huang, Experimental studies and constitutive modelling of the hardening of aluminium alloy 7055 under creep age forming conditions, International Journal of Mechanical Sciences 53(8) (2011) 595-605.
[20] Y.-L. Yang, A.C. Lam, Z. Shi, J. Lin, R. Said, Constitutive modelling of creep-ageing behaviour of peak-aged aluminium alloy 7050, MATEC Web of Conferences, EDP Sciences, 2015, p. 12008.
[21] Y. Li, Z. Shi, J. Lin, Y.-L. Yang, Q. Rong, B.-M. Huang, T.-F. Chung, C.-S. Tsao, J.-R. Yang, D.S. Balint, A unified constitutive model for asymmetric tension and compression creep-ageing behaviour of naturally aged Al-Cu-Li alloy, International Journal of Plasticity 89 (2017) 130-149.
[22] L. Cao, P.A. Rometsch, M.J. Couper, Clustering behaviour in an Al–Mg–Si–Cu alloy during natural ageing and subsequent under-ageing, Materials Science and Engineering: A 559 (2013) 257-261.
[23] I. Kalemba, C. Hamilton, S. Dymek, Natural aging in friction stir welded 7136-T76 aluminum alloy, Materials & Design 60 (2014) 295-301.
[24] K.S. Kumar, S.A. Brown, J.R. Pickens, Microstructural evolution during aging of an AlCuLiAgMgZr alloy, Acta Materialia 44(5) (1996) 1899-1915.
[25] J. Banhart, C.S.T. Chang, Z. Liang, N. Wanderka, M.D.H. Lay, A.J. Hill, Natural Aging in Al‐Mg‐Si Alloys – A Process of Unexpected Complexity, Advanced Engineering Materials 12(7) (2010) 559-571.
[26] L. Wu, W.G. Ferguson, Modelling of Precipitation Hardening in Casting Aluminium Alloys, Materials Science Forum, Trans Tech Publ, 2009, pp. 203-206.
[27] D.N. Seidman, E.A. Marquis, D.C. Dunand, Precipitation strengthening at ambient and elevated temperatures of heat-treatable Al (Sc) alloys, Acta Materialia 50(16) (2002) 4021-4035.
[28] J. Lin, J. Yang, GA-based multiple objective optimisation for determining viscoplastic constitutive equations for superplastic alloys, International Journal of Plasticity 15(11) (1999) 1181-1196.
[29] J. Cahoon, W. Broughton, A. Kutzak, The determination of yield strength from hardness measurements, Metallurgical Transactions 2(7) (1971) 1979-1983.
[30] N.E. Prasad, T.R. Ramachandran, Chapter 3 - Phase Diagrams and Phase Reactions in Al–Li Alloys, in: N.E. Prasad, A.A. Gokhale, R.J.H. Wanhill (Eds.), Aluminum-lithium Alloys, Butterworth-Heinemann, Boston, 2014, pp. 61-97.
[31] Y. Li, Z.S. Shi, Y.L. Yang, J.G. Lin, Investigation of Tensile and Compressive Creep Behaviour of AA2050-T34 during Creep Age Forming Process, Key Engineering Materials, Trans Tech Publ, 2016, pp. 323-330.